Faraday Discussions

A solid-state Li-air battery: computational studies of interfaces and relevance to discharge mechanism

Journal:	*Faraday Discussions*
Manuscript ID	FD-ART-04-2023-000083.R1
Article Type:	Paper
Date Submitted by the Author:	07-Jun-2023
Complete List of Authors:	Shan, Nannan ; Argonne National Laboratory, Materials Science Divison Ngo, Anh; University of Illinois at Chicago, Chemical Engineering Kondori, Alireza; Illinois Institute of Technology, Chemical & Biological Engineering ; Illinois Institute of Technology Asadi, Mohammad; Illinois Institute of Technology Curtiss, Larry; Argonne National Laboratory Materials Science Division

A solid-state Li-air battery: computational studies of interfaces and relevance to discharge mechanism

Nannan Shan,[1] Anh T. Ngo,[1,2] Alireza Kondari,[3] Mohammad Asadi,[3] Larry A. Curtiss[1]

[1] Materials Science Division, Argonne National Laboratory, Lemont, IL 60516 USA
[2] Department of Chemical Engineering, University of Illinois-Chicago 60607 USA
[3] Department of Chemical and Biological Engineering, Illinois Institute of Technology 60616 USA

There is much interest in developing new energy storage systems to replace currently available ones that mainly work based on Li ion intercalations. One attractive area is the Li-air battery for which most of the research has involved liquid electrolytes. There have been few studies of the use of a solid electrolyte in a Li-air battery. Recently, we reported the successful use of a solid-state electrolyte in a Li-air battery resulting in a Li_2O product and potentially much higher energy density than in a Li-air battery based on either a Li_2O_2 or LiO_2 product (Science 2023, **379**, 499). In this paper we discuss how the discharge mechanism involved in this solid-state Li-air battery differs from that of a Li-air battery with a liquid electrolyte. The solid-state mechanism is further explored with density functional studies of various interfaces involving the discharge product. We discuss the relevance of the results to the discharge mechanism in the solid-state Li-air battery.

Introduction

Lithium-oxygen (Li-O_2) batteries have drawn a much attention because of their potential high energy density compared to current Li-ion technologies based on intercalation.[1] A practical, cell level specific energy density between 1000 - 2000 W h kg^{-1} is potentially achievable with Li-O_2 systems. Generally, Li-O_2 batteries suffer from large electrochemical over-potentials and limited cycle life. The large charge overpotentials can result from electron transport limitations caused by the build-up of insoluble products on the cathode surface due to instabilities of the aprotic liquid electrolytes during discharge and charge, which can also severely limit the battery cycle life.

One approach to avoid the problems with liquid electrolytes in Li-O_2 batteries is to use a solid-state electrolyte. Although, there has been much research devoted to the development of solid-state-electrolytes for Li-ion batteries, very few attempts have been reported on the incorporation of solid state electrolytes in Li-O_2 batteries. One of the first reports was from Abraham et al[2] in 2010 who used a highly Li-ion conductive solid electrolyte membrane laminate fabricated from glass–ceramic and polymer–ceramic materials. The cell exhibited reversibility for about 40 cycles in a temperatire range of 30-105 C. They suggested that the results were promising for an ultra-

high energy density electrochemical source. In 2012 Kitaura and Zhou[3] reported on a solid-state lithium–air battery using a $Li_{1+x}Al_yGe_{2-y}(PO_4)_3$ inorganic solid electrolyte. The battery was successful in discharging and charging, but for only a few cycles and low capacity. Wang et al[4] reported solid-state Li–air battery based on an ultra-fine surface $Li_{1.5}Al_{0.5}Ge_{1.5}P_3O_{12}$ electrolyte. The battery was reversible for about 30 cycles with a polarization gap of more than 1 V. A recent paper[5] reported an integrated solid-state Li–air battery containing an ultrathin, high-ion-conductive lithium-ion-exchanged zeolite membrane integrated with cast lithium as the anode and carbon nanotubes. It also had an ionic liquid interface between the carbon nanotubes. The battery ran for about 150 cycles, more that the system without the protective zeolite on the anode. Several other reports of Li-air batteries using a solid-state electrolyte have been reported[6,7] but similar to the ones described above all showed fairly low reversibility and cyclability with Li_2O_2 as the main product.

We recently reported on a new ceramic-polymer electrolyte that has high ionic conductivity and mechanical stability as well as excellent compatibility and chemical stability at the interfaces of a Li-O_2 battery.[8] The solid electrolyte was composed of $Li_{10}GeP_2S_{12}$ (LGPS) nanoparticles in a polyethylene oxide (PEO)-LiTFSI matrix. A silane coupling agent, mPEO-TMS (3-[Methoxy(polyethyleneoxy)$_{6-9}$ propyl]trimethoxysilane) was added to form Si-S bonds with the LGPS nanoparticles. The Si-S coupling served to protect the LGPS nanoparticles from potential decomposition at the Li metal anode and the active cathode interfaces. The ionic conductivity of the ceramic polymer electrolyte (CPE) was 0.52 mS/cm at room temperature. This is about 10 times higher than that of the solid electrolyte (i.e., PEO/mPEO-TMS/LiTFSI) without LGPS nanoparticles. In addition, this new CPE has about about 15 times higher ionic conductivity than a PEO polymer electrolyte at room temperature. The CPE exhibits a large electrochemical redox stability window of 5.27 V and a transference number of 0.73.

The resulting solid state Li-air battery[8] showed excellent performance as it ran for over over 1000 cycles with a charge and discharge potentialsof 2.95 and 2.90 V vs. Li/Li^+, respectively, at the end of the first cycle. The potential gap increased from 50 mV at the first cycle to ~430 mV at the 1000th cycle. This cycling was done with a rate of 0.1 mA/cm^2 and a capacity of 0.1 mAh/cm^2. The cell operated in air at room temperature. The developed battery cell was tested at different

rates up to 0.5 mA/cm^2 and was found to operate, but the potential gap becomes larger with the higher rates.

The discharge product was characterized by several different techniques.[8] In situ Raman spectroscopic measurements showed that initially three products were being formed: LiO_2, Li_2O_2, and Li_2O. This was determined by identification of Raman peaks for each of the products. In addition, the *in situ* Raman results showed that the LiO_2 and Li_2O_2 intensities stopped growing after about one quarter of the discharge cycle while the Li_2O intensity continued to increase during all of the discharge cycle. These results suggested that the system attains a steady state when the amounts of LiO_2 and Li_2O_2 present remain constant as a source of oxygen (in the form of Li_2O_2) for the increasing amount of Li_2O. Titration results using several techniques indicated that the discharge product consisted of 98% Li_2O, 1% Li_2O_2, and 1% LiO_2. DEMs measurements were also consistent with a predominant Li_2O formation as it shows nearly a 4e per O_2 result. Ageing experiments in vaccum and in argon showed the LiO_2 Raman intensities decreased with time indicating that LiO_2 is in the outer layer of the discharge product, followed by Li_2O_2 with Li_2O in the interior. Finally, additional characterization including XRD and 3D-Raman also confirmed the presence of Li_2O.

This solid-state Li-air battery operates on an entirely new mechanism in which the discharge product results from a one-, two-, and four electron sequential reaction process resulting in predominant Li_2O formation deduced from the characterization results discussed above. In this paper we discuss the how the solid state mechanism differs from that in an aprotic liquid electrolyte-based Li-O_2 battery followed by a presentation of results of density functional calculations of some of the possible solid-solid interfaces that could be present in the discharge product and discussion of their relevance to the discharge mechanism.

Differences in solid- and liquid-electrolyte Li-O_2 battery discharge mechanisms

There are significant differences between the discharge mechanisms in liquid electrolyte-based Li-O_2 batteries and the solid-state one recently reported.[8] In this section we compare likely discharge mechanism in the two types of batteries, which result in different products. Simplified representations of what are believed to be the basic mechanisms in the two systems are illustrated in Figure 1. In the case of the liquid electrolyte there are two mechanisms illustrated, one for a solution phase mechanism and the other for a surface growth mechanism.

Solid-state electrolyte-based mechanism

First, we discuss the solid electrolyte Li-air battery mechanism postulated in Ref. 8 for the specific Li-air architecture used in that battery. This architecture has the solid-state electrolyte making limited contact with the cathode because of the roughness of the cathode as illustrated in Figure 1(a) with a closer view the interface illustrated in Figure 1(b). The mechanism is based on a sequential reaction interphase (SRI) illustrated in Fig. 1(c) and Scheme 1. This mechanism involves both gas-solid and solid-solid interfaces. After initiation and attainment of steady state of the discharge product growth, i.e., growth of Li_2O and constant small amounts of Li_2O_2 and LiO_2, there will be three interfaces: (1) The gas-solid interface involves the interface between air and the outermost component of the discharge product, LiO_2. The LiO_2 results from the one-electron reaction, i.e., $Li^+ + e + O_2 \rightarrow LiO_2$. The LiO_2 is the first product to be formed in the reaction sequence. (2) The second interface in the SRI is a solid-solid one and is between LiO_2 and Li_2O_2 with the latter product resulting from the addition of a second electron and cation to LiO_2, i.e., $LiO_2 + e + Li^+ \rightarrow Li_2O_2$. (3) The third interface in the SRI is also a solid-solid one and is between Li_2O_2 and Li_2O with the latter product resulting from the addition of two electrons and two cations to Li_2O_2, i.e., $Li_2O_2 + 2Li^+ + 2e \rightarrow 2Li_2O$. The electrons for the reactions occurring in the discharge product SRI come from the cathode while the Li cations come from the anode through the solid-state electrolyte.

The mechanism depends on the discharge product having high enough electronic and ionic conductivities. High ionic and electronic conductivities are likely since the discharge product is partially amorphous Li_2O,[8] which has been reported have much higher ionic and electronic conductivities than crystalline Li_2O. The ionic conductivity of amorphous Li_2O has been reported to be 10^{-7} S/cm and 10^{-5} S/cm in two experimental studies,[9],[10] while its electronic conductivity has been reported to be 10^{-8} S/cm.[9] Crystalline Li_2O has a much lower ionic conductivity of 10^{-12} S/cm and much lower electronic conductivity of $<10^{-14}$ S/cm from experiment.[11] In addition, although the LiO_2 and Li_2O_2 components are very small of the discharge product, they can also have high ionic and electronic conductivities if they are amorphous.[12]

We note that the interface between solid components may be a nanometer or more thick as shown in the calculations reported in the next section and they may be non-stoichiometric since conversion from one stoichiometry to the next will not occur at exactly the same instant in the

interface (Scheme 1), which may lead to defects that could contribute to enhanced conductivity. The charge mechanism is likely to be the reverse of the discharge mechanism shown in Scheme 1.

Liquid electrolyte-based mechanism

As mentioned earlier liquid electrolyte-based Li-O_2 batteries may have a variety of discharge mechanisms that result in different morphologies and components of product, usually LiO_2 and Li_2O. These have been the subject of many publications and they fall into two types: [13] solution phase growth and surface growth as illustrated in Figures 1(d) and 1(e). In the case of the solution phase mechanism the oxygen reduction occurs at a catalyst site on the cathode and the resulting superoxide reacts with a lithium cation in solution to form LiO_2. Once the electrolyte becomes supersaturated with LiO_2, nucleation and growth of LiO_2 on the surface occurs, which may be followed by disproportionation to Li_2O_2.[14] The latter can also occur in the electrolyte and lead to deposition of Li_2O_2. In the case of the surface growth mechanism the Li_2O_2 growth occurs by a two-electron reaction on the surface. This generally requires the Li_2O_2 to have good electronic conductivity and may limit the growth since bulk crystalline Li_2O_2 does not have good electronic conductivity. In both solution phase and surface growth the products are in almost always found to be either one- or two-electron reactions forming LiO_2 or Li_2O_2 or a mixture of them. The one exception to this is when molten salts are used as electrolytes, in which case Li_2O has been found to be a product,[15] but this requires higher temperatures because of the use of the molten salts.

It is of interest to consider why room temperature Li-O_2 batteries based on liquid electrolytes are limited to one- or two-electron Li + O_2 reactions, whereas the recently reported solid state Li-air battery resulted in a four-electron reaction forming Li_2O. The comparisons shown in Figure 1 provides an idea of what causes the difference. In the figure, we have indicated by the thickness of the arrows for Li^+, e- and O_2 the likely supply of these reactants to reaction sites. In the case of the liquid electrolyte Li^+ transport to the reaction site is probably limited due to the desolvation process and electron transport may be limited due to the solid/liquid interface electron transfer rate. In contrast for the solid-state Li-air battery the electron and cation transport to the reaction site are probably greater than the O_2 transport via LiO_2 and Li_2O_2 formation in the SRI. As a result, the $nLi^+ + ne + O_2$ reaction is forced to the four-electron result in the case of solid-state electrolyte. This can explain the predominance of Li_2O in the case of the solid-state Li-air battery as opposed to LiO_2 and Li_2O_2 in the case of the liquid electrolyte-based ones.

Calculations of interfacial structures

Computational methods

Spin-polarized density functional theory (DFT) calculations were carried out with Vienna Ab-initio Simulation Package (VASP).[16] The GGA-PBE functional[17] was adopted for exchange-correlation energy estimations. The first Brillouin zone was sampled with a k-mesh in Monkhorst-Pack scheme.[18] We employed the bulk structures of LiO_2, Li_2O_2 and Li_2O from our previous papers. [8,19] Cutoff energy for interface calculations were set to 400 eV with a 4×4×1 k-mesh.

The lattice constants of a LiO_2 bulk in Pnnm symmetry were converged to 2.96 Å, 3.94 Å and 4.92 Å. The optimized lattice constants for Li_2O_2 bulk in P63/mmc symmetry are a=b=3.16 Å, c=7.68 Å, α=β=90°, γ=120°, and for Li_2O in Fm3m space group a=b=c=4.63 Å, α=β= γ=90°. Due to the different symmetries of the bulk structures of LiO_2, Li_2O_2 and Li_2O, we used the most stable surfaces of them to build the interface model. Specifically, we used $LiO_2(101)$, $Li_2O_2(1\bar{1}00)$ and $Li_2O(110)$ surfaces because these surfaces models are all orthogonal. The thickness of LiO_2, Li_2O_2 and Li_2O in the interface structure are about 1.01 nm, 1.10 nm and 1.31 nm, respectively. For the optimization calculations of the interface, we fixed the most top and bottom periodic layers. We tested six different terminations for both the LiO_2-Li_2O_2 interface and the Li_2O-Li_2O_2 interface, and located the most stable configuration. In addition, we added two additional Li into the Li_2O-Li_2O_2 interface to evaluate the structure evolution during the discharge process when there is non-stoichiometry in the interface region. Furthermore, we calculated density of States (DOS) of Li_2O-Li_2O_2 interface with and without the additional Li using the HSE06 functional[20] since the GGA-PBE functional has been found to underestimate the band gap values for lithium oxides.[19]

Air/LiO_2 interface

The solid-state battery Li-air battery reported in Ref 8 has a porous Mo_3P/carbon cathode that allows air to enter the space between the cathode and the polymer/ceramic composite solid electrolyte. The space is created by the roughness of the Mo_3P cathode and the solid electrolyte. The heights of the peaks in the cathode as measured by atomic force microscopy range from about 200 to 500 nm. The roughness of the solid electrolyte was not measured. The solid electrolyte is assumed to contact the cathode material at its highest points. This is illustrated in Figure 1(a) and 1(b). The pores of the Mo_3P/carbon cathode for air transport are about 40 nm in diameter and appear to be still open after the discharge product is deposited on the surface of the cathode based on SEM imaging. As the discharge product grows the O_2 from the air will be in contact with the discharge product surface as illustrated in Fig. 1(c). The discharge product is likely to have LiO_2 on the surface Li_2O_2 and Li_2O underneath it based on ageing experiments mentioned

earlier. In Ref. 8 the binding energies of the O_2 on a LiO_2 surface were calculated using DFT. The binding energies of O_2 range from 0.2 to 0.7 eV on various sites on the Li(101) and Li(111) surfaces.

Thus, since chemical adsorption of O_2 at the air/LiO_2 interface is possible based on the calculations described above, electrons and Li cations available from the discharge product can react with the O_2 to form LiO_2. The Li cations and electrons for such a reaction should be available based on the ionic and electronic conductivities of various components of the discharge product as discussed previously. In calculations done for this paper we have investigated the binding energies a LiO_2 molecule on the LiO_2(101) surface. The binding energies of LiO_2 on the O- terminated LiO_2(101) and Li-terminated LiO_2(101) surfaces are 1.5 and 2.5 eV, respectively. The adsorption structures are shown in Figure 2. Thus, the air/LiO_2 interface should be amenable for addition of LiO_2 to the discharge product surface as required for the sequential reaction interphase concept discussed in Section II.

LiO_2/Li_2O_2 interface

We optimized six different configurations for the interface between LiO_2(101) and $Li_2O_2(1\bar{1}00)$ and the two most stable are shown in Figure 3(a). The structures show considerable disorder in the interface as denoted by the blue rectangles in Figure 3a. The disordered structure is on the order of about 0.8 nm in thickness. The calculations were done assuming that both LiO_2 and Li_2O_2 have crystalline structures. As mentioned previously there may be non-stoichiometry present in the discharge product at the interface between the LiO_2 and Li_2O_2 components. What we mean by this non-stoichiometry is illustrated in the reaction shown in Scheme 1 where partial addition of Li+ cations and electrons to LiO_2 units in the region of the interface will occur. As an example, we have added two Li in the supercell at the interface to make a stoichiometry of $Li_{1.75}O_2$. The optimized structure is shown in Figure 3b. This also results in an LiO_2/Li_2O_2 interface with disorder just as the ideal interface in Fig. 3a.

Li_2O_2/Li_2O interface

We optimized six different configurations for the interface between $Li_2O_2(1\bar{1}00)$ and Li_2O(110) and the two most stable interfaces are shown in Figure 4a. The structures show considerable disorder in the interface as denoted by the blue rectangles in the figure. The disordered structure is on the order of about 1.5 nm in thickness. As in the case of the LiO_2/Li_2O_2 interface the calculations were done assuming that both Li_2O_2 and Li_2O have crystalline structures. This is probably not the case since the characterization of Li_2O shows that it is in part amorphous. As mentioned previously there may be non-stoichiometry present in the discharge product at the interface between the Li_2O_2 and Li_2O components previous section for LiO_2 and Li_2O_2. As an example, we have added 2 Li to the supercell at the interface to make $Li_{2.75}O_2$.

After optimization, this interface becomes more disordered than that without 2 extra Li as shown in Figure 4b. In this interface some O are coordinated to 3 Li, oxygen is spin unpaired, and the Li-O distances are 1.8-1.9 A. This is different from the Li_2O_2 and Li_2O where the spins are paired and the coordination is higher. Thus, the Li_2O_2/Li_2O interface is likely to be disordered as in the case of the LiO_2/Li_2O_2 interface.

Since electronic conductivity is a key part of the discharge mechanism as discussed previously for the solid state Li-air battery we calculated the density of states for both the Li_2O_2/Li_2O interface as well as the same interface with two Li added as in 4(b). The calculated density of states with the HSE functional are shown in Figure 5. The introduction of the non-stoichiometry by addition of the two Li leads to a smaller band gap, suggesting a better electronic conductivity although more sophisticated computational studies are needed to confirm this.

Conclusions

There is much interest in developing new energy storage systems to eventually replace ones that are based on Li ion intercalation in a cathode material. One attractive area of research is the Li-O_2 battery where most of the papers have reported on systems involving liquid electrolytes. Despite the interest in solid state electrolytes for Li-ion batteries, there have been few studies of the use of a solid electrolyte in Li-O_2 batteries. In this paper we first reviewed our successful use of a solid-state electrolyte in a Li-air battery that results in a Li_2O product and has a potentially much higher energy density than in a Li-air battery based on either a Li_2O_2 of LiO_2 product.[8] In this paper we provided a possible explanation for why the discharge mechanism involved in this solid-state Li-air battery appears to depend on fast ionic and electronic transport through the discharge product. This likely differs from that of a Li-air battery with a liquid electrolyte where ionic transport is limited by ion desolvation in the liquid electrolyte and electronic conductivity by electron transfer at the liquid/cathode interface. The solid-state mechanism is further explored with density functional studies of various interfaces involving the discharge product. The results indicate that these interfaces are disordered and can contribute to the enhanced conductivity of the discharge product required for formation of Li2O in the sequential reaction interphase in the solid-state Li-air battery.

References

1 Z. Ma, X. Yuan, L. Li, Z. F. Ma, D. P. Wilkinson, L. Zhang and J. Zhang, *Energy Environ Sci*, 2015, **8**, 2144.

2 B. Kumar, J. Kumar, R. Leese, J. P. Fellner, S. J. Rodrigues and K. M. Abraham, *J Electrochem Soc*, 2009, **157,** A50.

3 H. Kitaura and H. Zhou, *Energy Environ Sci*, 2012, **5**, 9077.

4 S. Wang, J. Wang, J. Liu, H. Song, Y. Liu, P. Wang, P. He, J. Xu and H. Zhou, *J Mater Chem A Mater*, 2018, **6**, 21248.

5 X. Chi, M. Li, J. Di, P. Bai, L. Song, X. Wang, F. Li, S. Liang, J. Xu and J. Yu, *Nature*, 2021 **592**, 551.

6 S. Hasegawa, N. Imanishi, T. Zhang, J. Xie, A. Hirano, Y. Takeda and O. Yamamoto, *J Power Sources*, 2009, **189**, 371.

7 X. Zhu, T. Zhao, P. Tan, Z. Wei and M. Wu, *Nano Energy*, 2016, **26**, 565.

8 A. Kondori, M. Esmaeilirad, A. M. Harzandi, R. Amine, M. T. Saray, L. Yu, T. Liu, J. Wen, N. Shan, H. H. Wang, A. T. Ngo, P. C. Redfern, C. S. Johnson, K. Amine, R. Shahbazian-Yassar, L. A. Curtiss and M. Asadi, *Science* 2023*,* **379**, 499.

9 S. D. Han, K. N. Wood, C. Stetson, A. G. Norman, M. T. Brumbach, J. Coyle, Y. Xu, S. P. Harvey, G. Teeter, A. Zakutayev and A. K. Burrell, *ACS Appl Mater Interfaces*, 2019, **11**, 46993.

10 S. Lorger, K. Narita, R. Usiskin and J. Maier, *Chemical Communications*, 2021, **57**, 6503.

11 S. Lorger, R. Usiskin and J. Maier, *J Electrochem Soc*, 2019, 166, A2215.

12 Y. Zhang, Q. Cui, X. Zhang, W. C. McKee, Y. Xu, S. Ling, H. Li, G. Zhong, Y. Yang and Z. Peng, *Angewandte Chemie - International Edition*, 2016, **128**, 10875.

13 L. Johnson, C. Li, Z. Liu, Y. Chen, S. A. Freunberger, P. C. Ashok, B. B. Praveen, K. Dholakia, J. M. Tarascon and P. G. Bruce, *Nat Chem*, 2014, **6**, 1091.

14 M. J. Welland, K. C. Lau, P. C. Redfern, L. Liang, D. Zhai, D. Wolf and L. A. Curtiss, *Journal of Chemical Physics*, 2015, 143, 224113.

15 C. Xia, C. Y. Kwok and L. F. Nazar, *Science,* 2018, **361**, 777.

16 G. Kresse and J. Furthmüller, *Comput Mater Sci*, 1996, **6**, 15.

17 J. P. Perdew, K. Burke and M. Ernzerhof, *Phys Rev Lett*, 1996, **77**, 3865.

18 H. J. Monkhorst and J. D. Pack, *Phys Rev B*, 1976, **13**, 5188.

19 K. C. Lau, L. A. Curtiss and J. Greeley, *Journal of Physical Chemistry C*, 2011, **115**, 23625.

20 J. Heyd, G. E. Scuseria and M. Ernzerhof, *Journal of Chemical Physics,* 2003, **118**, 8207

Acknowledgements

Work supported by the U.S. Department of Energy under Contract DE-AC02-06CH11357 from the Vehicle Technologies Office, Office of Energy Efficiency and Renewable Energy and the Joint Center for Energy Storage Research (JCESR), an Energy Innovation Hub funded by the Office of Science, Basic Energy Sciences.

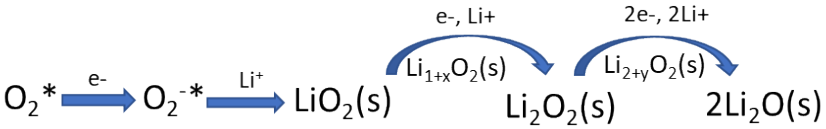

Scheme 1. Sequential reactions of O_2, electrons (e^-) and lithium cations (Li^+) leading to Li_2O formation.

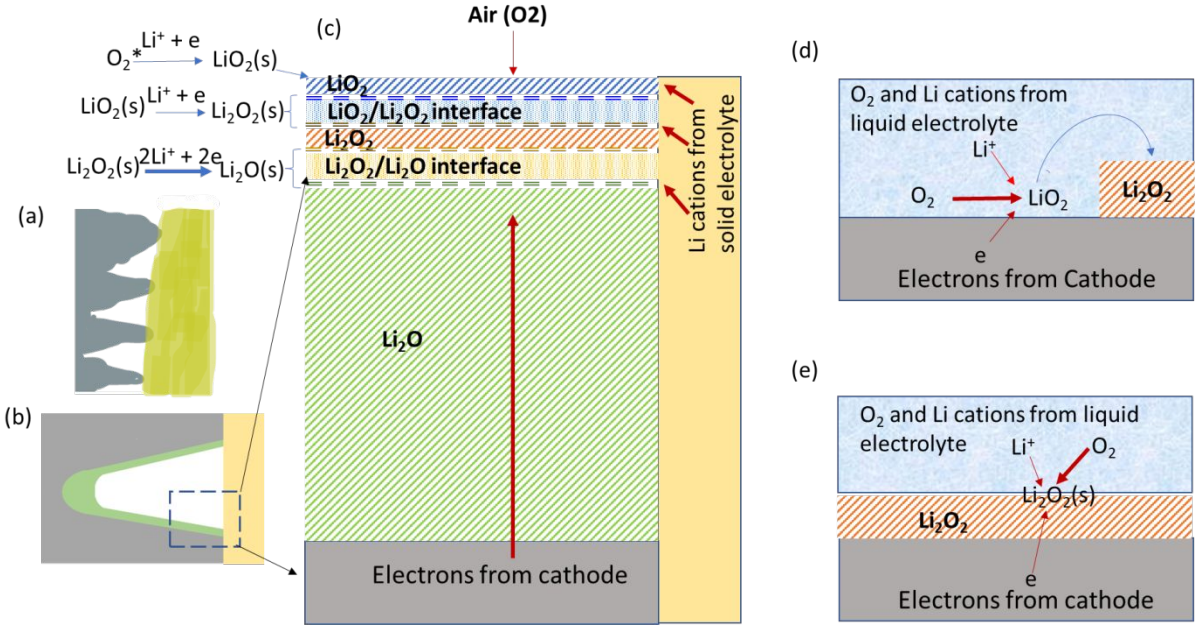

Figure 1. Postulated growth mechanisms for solid state Li-air battery in comparison with liquid electrolyte-based Li-air batteries. (a) Illustration of the cathode (gray)/solid electrolyte (yellow) interface. (b) Illustration of one "valley" of the cathode (gray)/solid electrolyte (yellow) interface with discharge deposit (light green) in the "valley". (c) Idealized sequential reaction interphase (SRI) with interfaces in a solid-state Li-air battery. (d) Illustration of solution phase growth in a liquid electrolyte-based Li-air battery. (e) Illustration of surface growth in a liquid electrolyte-based Li-air battery.

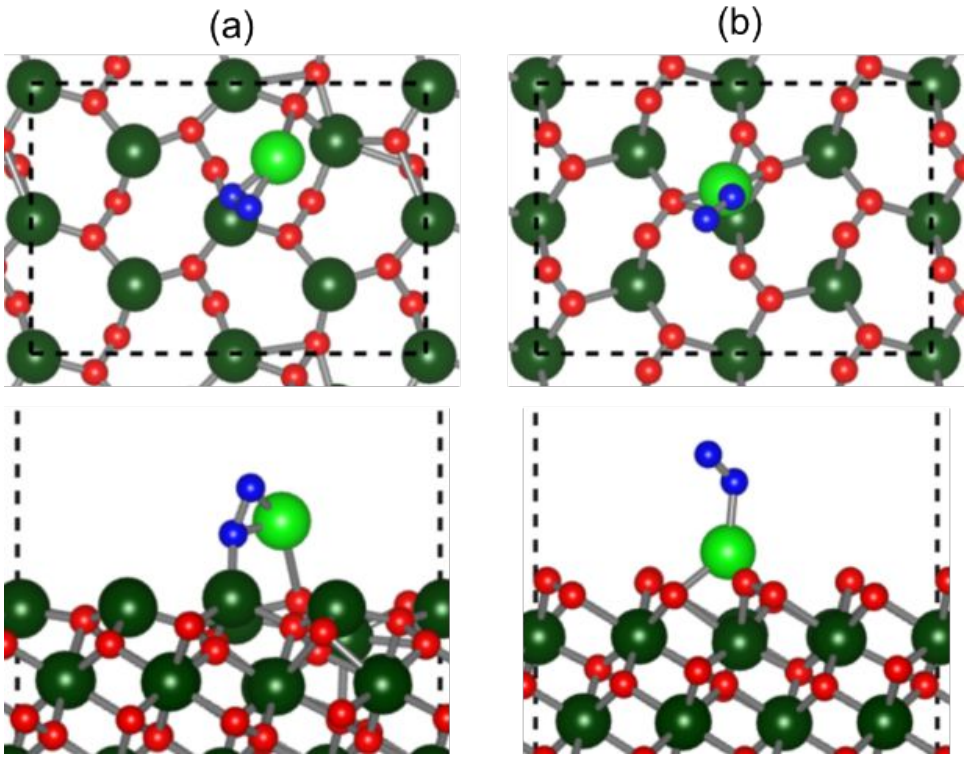

Figure 2. Adsorption structures of LiO_2 on the (a) Li- terminated LiO_2(101) and (b) O-terminated LiO_2(101) surfaces. Atom colors: Li (green), O (red) for the LiO_2 surface; Li (light green); O (blue) for the LiO_2 molecule.

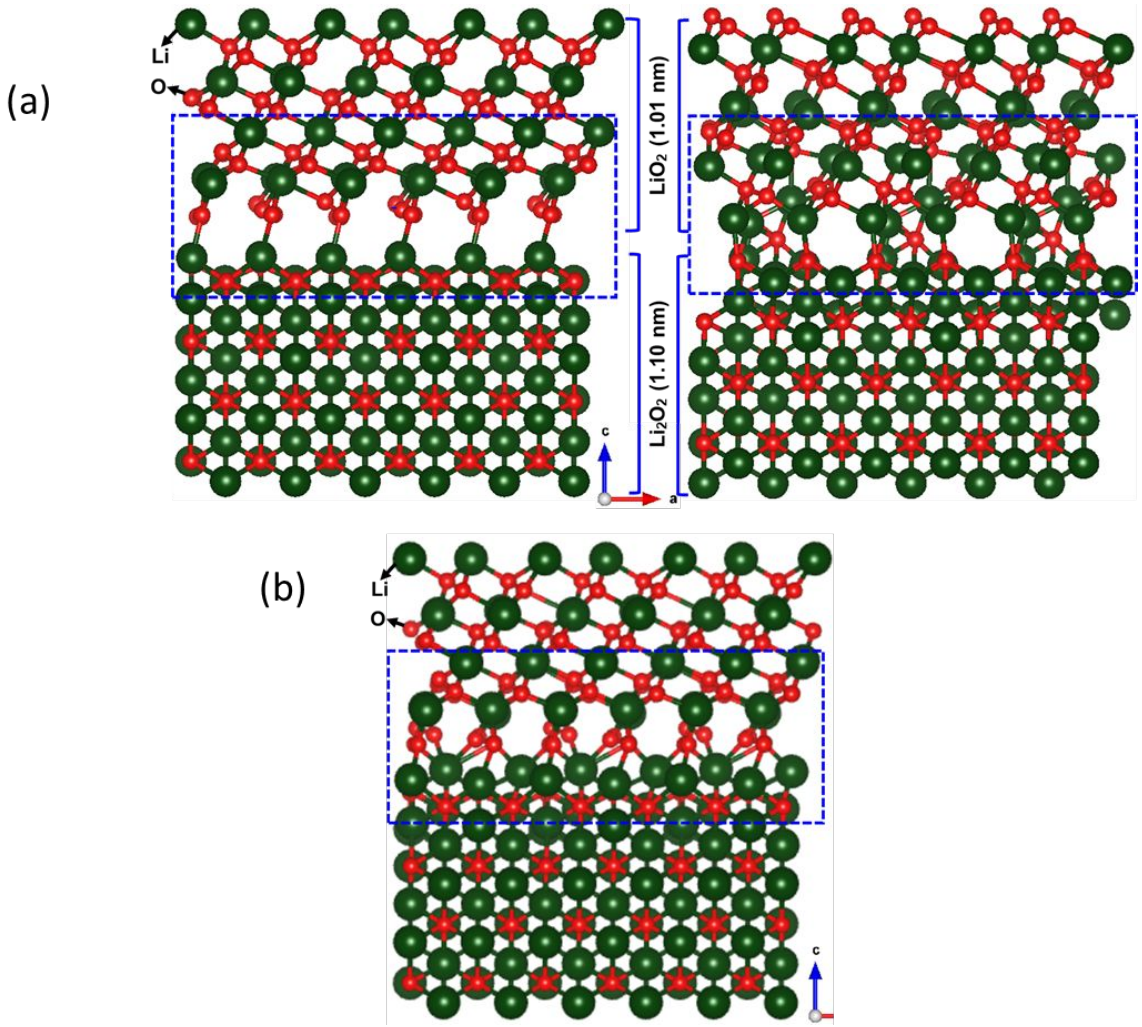

Figure 3. (a) Structures of the two most stable LiO_2/Li_2O_2 interfaces of the six investigated. Most stable structure is on the left. (b) Structure of the most stable LiO_2/Li_2O_2 interface with two Li added to the supercell.

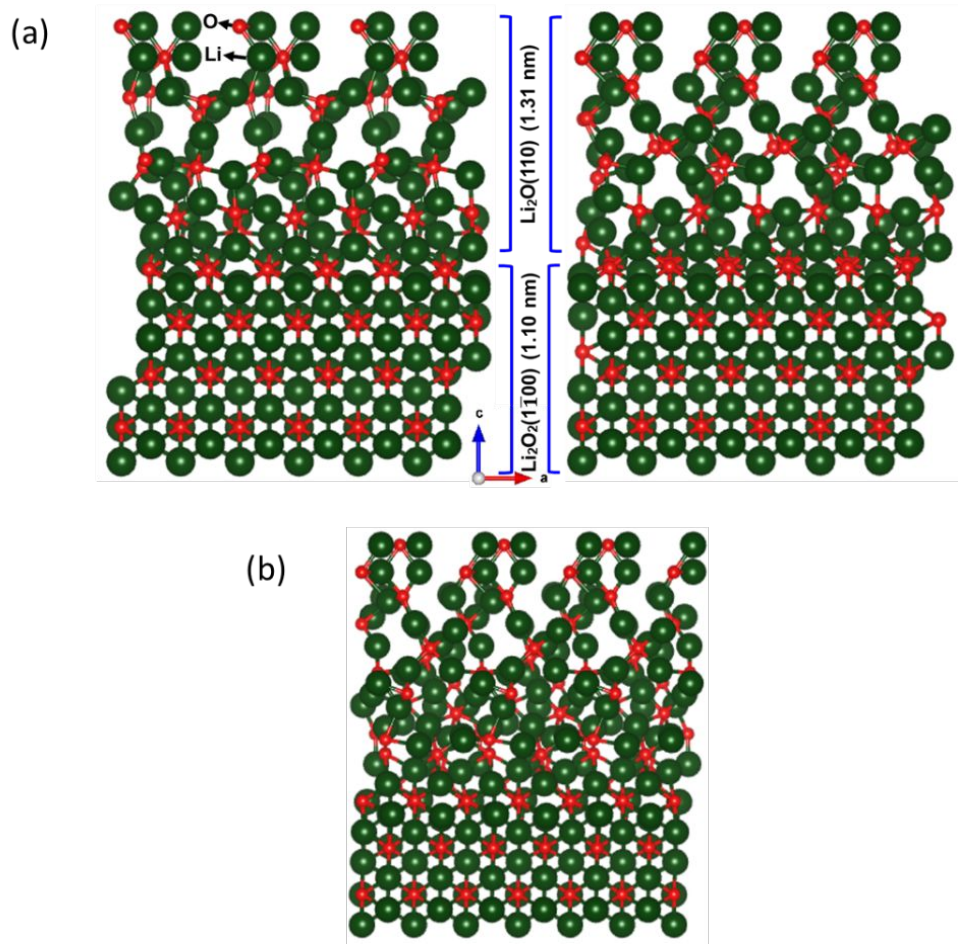

Figure 4. (a) Structures of the two most stable Li_2O_2/Li_2O interfaces of the six investigated. Most stable structure is on the left. (b) Structure of the most stable Li_2O_2/Li_2O interface with two Li added to the supercell.

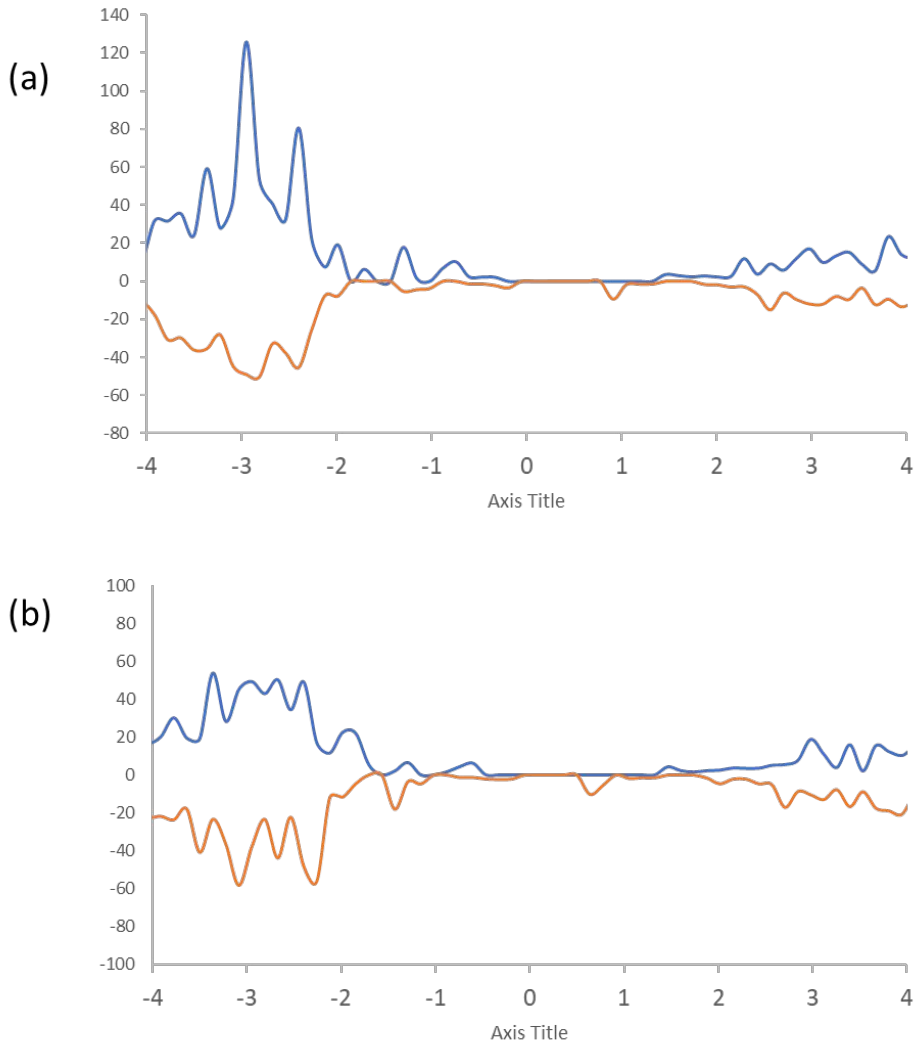

Figure 5. (a) Density of states of the most stable Li_2O_2/Li_2O interface. (b) Density of states of the most stable Li_2O_2/Li_2O interface with two Li added to the supercell. Both calculations used the HSE06 functional.